Contactless Blood Pressure Estimation using infrared video from facial and hand regions

Thomas Stogiannopoulos, Nikolaos Mitianoudis

Electrical & Computer Engineering Dep.
Democritus University of Thrace
Xanthi, Greece
{tstogian, nmitiano}@ee.duth.gr

***Abstract*—This study investigates the potential of using low-cost infrared cameras for non-contact monitoring of blood pressure (BP) in humans. Previous research has shown that robust contactless BP monitoring using RGB cameras is possible. In this study, the Eulerian Video Magnification (EVM) technique is employed to enhance minor variations in skin pixel intensity in the forehead and palm regions captured by an infrared camera. The primary focus of this study is to explore the possibility of using infrared cameras for contactless BP monitoring under low-light or nighttime conditions. Results show that the proposed approach has surpassed the stringent accuracy standards set forth by the British Hypertension Society (BHS) and the Association for the Advancement of Medical Instrumentation (AAMI) protocol.**

***Index Terms*—Blood Pressure, Hypertension, Generalized Additive Model (GAM), iPPG**

I. Introduction

Contactless measurement techniques have made significant breakthroughs recently in the monitoring of several physiological parameters, including heart rate, oxygen saturation and blood pressure. Most importantly, contactless measuring techniques are non-invasive and therefore eliminate the risk of infection and discomfort, compared to more commonly-used invasive procedures. More specifically, contactless measurement techniques have even more significant benefits for the elderly. Aging is often accompanied with a decline in health and functional status, making the elderly more prone to age-related diseases, including cardiovascular diseases [1].

Hypertension and hypotension are two medical conditions that are related to blood pressure levels. Blood pressure is the force exerted by circulating blood against the walls of the blood vessels. Hypertension refers to a condition where elevated blood pressure occurs frequently, while hypotension refers to the contrary condition, where low blood pressure is more frequently observed. Thus, tracking blood pressure levels is imperative for elderly people due to the increased frequency of these conditions and their association with other important health risks. Hypertension, also known as "high" blood pressure, is defined as a systolic blood pressure (SBP) of 130 mmHg or higher or a diastolic blood pressure (DBP) of 80 mmHg or higher [2]. This condition is a leading risk factor for cardiovascular diseases, such as stroke, heart attack, heart failure, and kidney disease. Hypertension can result from multiple factors, such as genetic predisposition, unhealthy lifestyle choices, and age-related changes in blood vessel function [3]. More specifically, for the elderly population, hypertension is highly prevalent and has distinct characteristics compared to younger population. Statistics show that almost 46% of adults in the United States have hypertension [2]. Human blood vessels become stiffer due to aging, and thus the risk of developing hypertension is more prevalent in older people [4]. Hypertension in older adults is also associated with a higher risk of cardiovascular events, cognitive decline, kidney disease, and unfortunately mortality [5].

Hypotension is officially defined as a systolic blood pressure below 90 mmHg or a diastolic blood pressure below 60 mmHg [6]. Elderly people, diagnosed with hypertension, may experience transient hypotensive episodes, which essentially translate to temporary drops in blood pressure that can cause significant clinical implications. These episodes may indicate compromised blood flow to vital organs including the brain and heart, and they can be associated with acute cardiovascular and cerebrovascular incidents [7]. Thus, BP monitoring is essential for tracking hypertension or hypotension incidents in elderly as well as normal people.

A contactless system is based on optical techniques, such as image photoplethysmography (iPPG) and remote photoplethysmography (rPPG), that can capture physiological signals from the skin's surface. Consequently, the use of contactless methods minimizes the psychological and physiological stressors. Contactless measuring techniques also offer the advantage of continuous monitoring, which allows for real-time monitoring of physiological parameters, without the need for frequent interruption of the person's everyday life. This can be particularly helpful for critically-ill patients, who require constant vital-sign monitoring.

Prior research has been particularly dedicated to the investigation of contactless methods for blood pressure estimation and monitoring [20], [26]–[29]. Most of these techniques involve the use of an RGB camera in the capturing process. In contrast, our approach distinguishes itself through the utilization of an infrared camera in conjunction with motion magnification. There have been contactless methods, primarily based on facial signals [26], [28], [29] or, in some cases, the combined utilization of facial and raised hand signals [20], [27].

This study attempts to quantify the feasibility of using single-channel infrared videos of facial and hand regions for accurate blood pressure estimation. The motivation behind this research is the potential benefits offered by the single-channel infrared wavelength, such as reduced computational complexity, lower hardware requirements, and immunity to varying light conditions (day, evening or night). Our goal is to enhance eldercare by providing healthcare professionals with a reliable tool for unobtrusive and accurate blood pressure monitoring. This methodology demonstrates a high degree of adaptability for integration within hospital and health clinic settings, particularly in non-ICU (intensive care units) where monitoring capabilities may be constrained.

II. Proposed Methodology

A. Facial & Palmar Segmentation

It is common in contactless BP monitoring to process signals extracted from two body regions. Commonly with other approach, we chose to use the face and hand regions of the body in order to extract signals useful for BP measurement.

The forehead region was deliberately chosen, due to its well-established association with reliable cardiovascular signals, including pulse rate and blood flow. Simultaneously, the upper palm region was also selected for blood pressure estimation, mainly due to the fact that its consistent blood supply, provided by the superficial palmar arch [31], and stable skin characteristics contribute to its stability for contactless blood pressure estimation.

At first, we employed OpenCV's deep learning Single Shot Detector (SSD) model, as a fundamental component of our facial detection process in the captured video clip. The next step was to isolate the forehead region. The isolation process is facilitated by utilizing standard ratios between essential face landmarks typically found in the average human face, as elaborated in more detail in [8]–[10]. In our previous work [25], we described the process of isolating the forehead region through the employment of several equation that were derived from the standard ratios between essential face landmarks. This constituted a stable framework to accurately extract and segregate the forehead region from the remaining face.

Next, we use a hand detection framework, which allows to track hand landmarks in an image. The mediapipe approach [11] infers 21 3D keypoints of a hand from a single frame, enabling real-time hand and finger tracking. Figure 1 visually demonstrates the accurate and precise localization of 21 3D hand-knuckle coordinates [11]. In the context of this application, our primary focus lies in the specific area formed by the landmarks 0, 1, 5, 9, 13, and 17. These key landmarks serve as critical reference points, precisely marking the boundaries and spatial extent of the upper palm area that is relevant for our analysis.

B. Post-Processing & Peak Detection

For every recorded video segment we focus on the forehead and palm regions. The next step involves the application of the Eulerian Video Magnification (EVM) technique [12] is

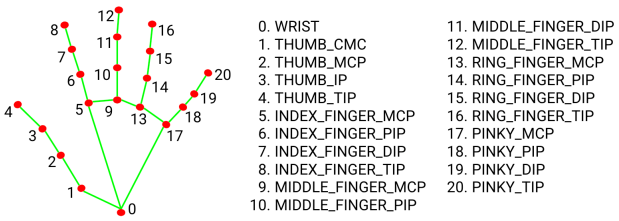

Fig. 1. The analytical localization of 21 3D hand-knuckle coordinates by the mediapipe approach.

employed to enhance minor variations within the frequency spectrum of 0.4 to 4 Hz. The primary objective of this procedure is to eliminate unwanted noise and artifacts from the signal and boost non-visible information. Consequently, we compute both the mean and standard deviation metrics for each individual frame in order to quantify the temporal characteristics of the physiological signals embedded within the video sequences. This yields two time series for the forehead and two for the palm region.

Next, we must detect and compare the position of similar discrete between the signals extracted from the forehead and the palm region. Two peaks in the forehead and the palm region that are correlated constitute a peak pair. A discerning criterion is applied whereby pairs of detected peaks, should their temporal separation exceed 5 frames, are omitted from further consideration. Drawing inspiration from the work of Fan et al. [20], who similarly endeavored to compute pulse transit time between facial and palm regions, we recognize that pulse transit time spans a range of approximately 60 milliseconds (ms) in their study. Our methodology involves the systematic accumulation of median time intervals among peak pairs for each individual video recording. Subsequently, an averaging procedure is employed to compute the mean value of these individual median time intervals across all video recordings within a given volunteer's dataset. Ultimately, a comprehensive summation of our investigative process results in the derivation of dual definitive measurements per individual volunteer. The objective therein is the formulation and refinement of two distinctive functions, each characterized by a dual-input configuration via regression. Specifically, we endeavor to construct a two-input function tailored to prognosticate systolic blood pressure, and another one for diastolic blood pressure.

C. Generalized Additive Models

This study delves into the utilization of Generalized Additive Models (GAM) for regression, as discussed by Hastie et al [30]. The primary contrast between a GAM and conventional Generalized Linear Models, such as Linear Regression, lies in the fact that GAMs have the capacity to capture non-linear connections between independent and dependent variables. Unlike Generalized Linear Models, GAMs can furnish regression outcomes that involve the summation of multiple adaptable functions for each feature, known as splines. These splines are intricate non-parametric functions

that unveil the non-linear aspects inherent in each feature. Consequently, a GAM allows the interpretation of a random variable Y's inference as the sum of predictive random variables $X_1, X_2, \ldots, X_p$, as formulated below:

$$\mathcal{E}\{Y|X_1, X_2, \ldots, X_p\} = f_0 + \sum_{j=1}^{p} f_j(X_j) \tag{1}$$

Here, the functions $f_j(\cdot)$ represent smooth nonparametric functions that are standardized to ensure that $\mathcal{E}\{f_j(X_j)\} = 0$, following Hastie et al.'s work [30]. GAMs are especially well-suited for regression tasks due to their ability to comprehend nonlinear associations and trends, while retaining the advantage that the impact of an individual variable remains uninfluenced by the values of other variables. The framework of GAMs also empowers us to modulate the smoothness of predictor functions, effectively preventing the risks of overfitting.

D. Polynomial Regression

Linear Regression, Quadratic Regression, and Cubic Regression are fundamental statistical techniques that serve as powerful tools for modeling and analyzing the relationships between variables in empirical data, each offering distinct degrees of complexity and flexibility.

Linear Regression entails fitting a straight line to the data points, thus establishing a linear relationship between the independent (predictor) variable, usually denoted as x, and the dependent (response) variable, typically denoted as y. The equation takes the form:

$$y = \beta_0 + \beta_1 x + \varepsilon \tag{2}$$

where β_0 is the intercept, β_1 is the slope, and ε represents the residual error. The goal is to find the best-fit line that minimizes the sum of squared residuals, effectively capturing the overall trend between the variables.

Quadratic Regression, building upon the foundation of Linear Regression, introduces curvature to the model by incorporating a quadratic term. The equation becomes:

$$y = \beta_0 + \beta_1 x + \beta_2 x^2 + \varepsilon \tag{3}$$

where β_2 represents the coefficient of the quadratic term. This technique accommodates situations where the relationship between variables is more nuanced, potentially exhibiting a parabolic pattern (upward or downward curvature).

Cubic Regression further extends the repertoire by incorporating cubic terms, enabling the representation of even more intricate curves within the data. The equation takes the form:

$$y = \beta_0 + \beta_1 x + \beta_2 x^2 + \beta_3 x^3 + \varepsilon \tag{4}$$

where β_3 signifies the coefficient of the cubic term. This technique is invaluable when the underlying relationship demonstrates pronounced curvature, including scenarios where the data follows an "S" or "U" shaped trajectory.

III. Experiments

In order to assess the performance of the proposed method for estimating systolic and diastolic blood pressure, a dataset of infrared videos with blood pressure measurements was created in which fifteen (15) participants took part. The reference point for each participant's blood pressure was a clinically validated commercial automatic upper arm blood pressure monitor (Omron M6 Comfort (HEM-7360-E)) that monitored the blood pressure levels continuously throughout the trials. All the subjects were filmed in a room with natural sunlight using an infrared camera. We employed a carefully designed approach that involved taking three consecutive readings within a span of two minutes, with a 30-second interval between each measurement, totalling 3 minutes. The participants were instructed to remain as motionless as possible during the recordings. To avoid potential registration issues, the participants were seated at a fixed distance from the camera, strategically chosen to include the forehead region and the upper palm region within the field of view. All data and blood pressure reference values are publicly available and can be found on the paper's GitHub page.

In this study, we utilized a wired Google Nest Cam to record video footage of the participants. The camera settings were configured to "Infrared Always" mode, providing a resolution of 1920×1080 Full HD and a frame rate of 30 fps. To minimize potential distortion caused by the camera's wide-angle lenses, the camera was positioned at eye level, maintaining a distance of 85 cm from the participants. To obtain the video clips, the researchers downloaded them from Google's Cloud service, where they had been uploaded. It is important to note that the video clips obtained from the cloud service contained compression noise, which had the potential to impact the accuracy of the process. Despite the presence of compression noise in the video clips, the proposed approach still yielded satisfactory results, thereby validating the proof of concept put forth by this study.

Motion magnification tasks were executed using MATLAB R2018b, primarily due to the availability of the original motion magnification code by Wu et al. [12] in MATLAB. On the other hand, the proposed machine learning regression approaches were implemented using Python v3.8.10, employing the scikit-learn package. For the face/hand detection and segmentation algorithm, Python v3.10.8 was employed. For conducting the experiments, we utilized a high-performance Ubuntu 22.04 PC equipped with 64GB RAM, an Intel i9 2.5 GHz 16-Core CPU, and an NVIDIA GeForce RTX 3090 GPU with 24GB of RAM [1].

A. Validation Standards

The American Association for the Advancement of Medical Instrumentation (AAMI) and the British Hypertension Society (BHS) have independently published comprehensive standards pertaining to sphygmomanometers, encompassing rigorous protocols for evaluating the accuracy and performance of

[1]The developed code can be found at [32]

TABLE I
GRADING CRITERIA EMPLOYED BY THE BRITISH SOCIETY OF HYPERTENSION (BSH)

Model	$\leqslant 5$ **mm Hg**	$\leqslant 10$ **mm Hg**	$\leqslant 15$ **mm Hg**
A	60%	85%	95%
B	50%	75%	90%
C	40%	65%	85%
D	$\leqslant 40$	$\leqslant 65$	$\leqslant 85$

TABLE II
MODELS' ACCURACY REGARDING SYSTOLIC BLOOD PRESSURE (TOP) & DIASTOLIC BLOOD PRESSURE (BOTTOM) USING BSH PROTOCOL

	$\leqslant 5$ **mm Hg**	$\leqslant 10$ **mm Hg**	$\leqslant 15$ **mm Hg**
Linear Regression	20%	53.33%	66.67%
Quadratic Regression	60%	60%	86.67%
Cubic Regression	80%	93.33%	100%
GAM	58%	92.35%	100%
Linear Regression	40%	86.67%	93.33%
Quadratic Regression	66.67%	100%	100%
Cubic Regression	80%	100%	100%
GAM	68.4%	100%	100%

these medical devices [13], [14]. The BHS protocol assigns grades to devices based on their agreement with the mercury standard for systolic and diastolic pressures. The highest level of agreement is denoted by grade A, while the lowest level is indicated by grade D. For a sphygmomanometer to fulfill the BHS protocol, it must achieve at least grade B for both systolic and diastolic readings, reflecting a clinically acceptable level of accuracy and agreement with the mercury standard [14]. Similarly, the American Association for the Advancement of Medical Instrumentation (AAMI) has formulated its own evaluation criteria for sphygmomanometers. According to the AAMI protocol, the test device's measurements should closely match the mercury standard, with a mean difference from the standard not exceeding 5 mm Hg for blood pressure readings. Additionally, the standard deviation, which represents the variability of differences between the test device and the mercury standard, should not exceed 8 mm Hg [13]. Compliance with both of these standardized criteria provides confidence in the reliability of these medical devices for blood pressure measurement. It is noteworthy that not all examined papers incorporate both accuracy protocols; certain studies utilize both protocols [26], while others exclusively employ one of the two [20], [28], [29], with a preference for the AAMI protocol.

B. Results

Through experimentation, we evaluated four distinct regression models, and our findings reveal that the Cubic and Generalized Additive Model (GAM) regression models have demonstrated consistent adherence to the established criteria outlined by both the British Hypertension Society (BSH) and the Association for the Advancement of Medical Instrumentation (AAMI) protocols. Notably, the substantial R^2 scores attained by these models serve as robust indicators of the considerable correlation achieved between the estimated blood pressure values and the reference standards, thereby substantiating the efficacy and potential clinical relevance of our approach. Detailed results and model performance metrics are provided in Table II and III.

TABLE III
MODELS' ACCURACY REGARDING SYSTOLIC BLOOD PRESSURE (TOP) & DIASTOLIC BLOOD PRESSURE (BOTTOM) USING AAMI PROTOCOL

Model	MAE	SD	R^2 **Score**
Linear Regression	12.01	8.43	0.1664
Quadratic Regression	7.04	5.41	0.6948
Cubic Regression	3.8	3.11	0.9068
GAM	4.99	3.37	0.8598
Linear Regression	6.38	3.91	0.2311
Quadratic Regression	3.86	2.71	0.6944
Cubic Regression	2.08	2.33	0.8658
GAM	4.03	2.48	0.6924

IV. CONCLUSIONS

Our study has effectively demonstrated ample evidence supporting the feasibility of contactless, non-invasive blood pressure monitoring utilizing data derived from a single-channel infrared stream. The method put forth in this study leverages precise facial and palmar segmentation, combined with the technique of motion magnification. Through this approach, we successfully deduce the pulse transit time between the corresponding signals acquired from each video within our dataset. This transit time data is further aggregated and analyzed to compute the average transit time specific to each participant. Leveraging an array of regression tools, the obtained results were subjected to validation against internationally recognized health protocols, exceeding the stipulated criteria. This approach lends itself readily to potential application within a hospital or healthcare clinic setting.

V. ACKNOWLEDGMENT

This study was made possible through the project "Improvement of the Quality of Life and Activity for the Elderly" (MIS 5047294) which was implemented under the "Support for Regional Excellence" program, financed by the "Competitiveness, Entrepreneurship and Innovation" program (NSRF 2014-2020) and funded jointly by Greece and the European Union (European Regional Development Fund). We would like to extend their appreciation to all participants who volunteered for the study.

REFERENCES

[1] Z. Li, Z. Zhang, Y. Ren et al. Aging and age-related diseases: from mechanisms to therapeutic strategies. Biogerontology 22, 165–187 (2021).
[2] P. Muntner, D. Shimbo, R.M. Carey, J.B. Charleston, T. Gaillard, S. Misra, M.G. Myers, et al. "Measurement of Blood Pressure in Humans: A Scientific Statement from the American Heart Association." Hypertension 73, no. 5 (March 4, 2019).
[3] S. Cheng, V. Xanthakis, L.M. Sullivan, and R.S. Vasan. "Blood Pressure Tracking over the Adult Life Course." Hypertension 60, no. 6 (October 29, 2012): 1393–99.

[4] T.W. Buford, “Hypertension and Aging.” Ageing Research Reviews 26 (February 1, 2016).

[5] E. Oliveros, H. Patel, S. Kyung, S. Fugar, A. Goldberg, N. Madan, and K.A. Williams. “Hypertension in Older Adults: Assessment, Management, and Challenges.” Clinical Cardiology 43, no. 2 (December 11, 2019)

[6] E. Magny, C. Donadio, F. Maronnat, D. Nghiem, E. Berthelot, J. Belmin, and C. Lafuente-Lafuente. “Hypotensions in the Elderly: Clinical and Therapeutic Features.” La Presse Médicale 48, no. 2 (February 3, 2019).

[7] S.A. Ermasova, and Y.G. Shvarts. “Transient Hypotension in Elderly Hypertensive Patients: What and How to Manage?” e-Journal of Cardiology Practice 22 (February 2, 2022).

[8] J. Milutinovic, K. Zelic, and N. Nedeljkovic. “Evaluation of Facial Beauty Using Anthropometric Proportions.” The Scientific World Journal, pp. 1–8., 2014.

[9] K.S. Kaya, B. Türk, M. Cankaya, N. Seyhun, and B. Uslu Coşkun. “Assessment of Facial Analysis Measurements by Golden Proportion.” Brazilian Journal of Otorhinolaryngology, Vol. 85, No. 4, pp. 494–501, 2019.

[10] J. W. Fernandes. “The Legacy of Art in Plastic Surgery.” Plastic and Reconstructive Surgery - Global Open, Vol. 9, No. 4, 2021.

[11] Mediapipe Hands (2023) GitHub. Available at: https://github.com/google/mediapipe/blob/master/docs/solutions/hands.md (Accessed: 13 August 2023).

[12] H.Y. Wu, M. Rubinstein, E. Shih, J. Guttag, F. Durand, and W. Freeman. “Eulerian Video Magnification for Revealing Subtle Changes in the World.” ACM Trans. on Graphics, Vol. 31, no. 4, pp. 1–8, 2012.

[13] W.B. White, A.S. Berson, C. Robbins, M.J. Jamieson, L.M. Prisant, E. Roccella, and S.G. Sheps. “National Standard for Measurement of Resting and Ambulatory Blood Pressures with Automated Sphygmomanometers.” Hypertension 21, no. 4 (1993): 504–9.

[14] E. O’Brien, et al. The British Hypertension Society protocol for the evaluation of blood pressure measuring devices: Jour. of Hypertension 1993, 11 (Suppl 2): S43-S62.

[15] C. Garratt, D. Ward, A. Antoniou, and A. J. Camm. “Misuse of Verapamil in Pre-Excited Atrial Fibrillation.” The Lancet, Vol. 333, no. 8634, pp. 367–69, 1989.

[16] L. Kong, Y. Zhao, L. Dong, Y. Jian, X. Jin, B. Li, Y. Feng, M. Liu, X. Liu, and H. Wu, “Non-Contact Detection of Oxygen Saturation Based on Visible Light Imaging Device Using Ambient Light.” Optics Express, Vol. 21, No. 15, 2013.

[17] A. de Fátima Galvão Rosa and R.C. Betini. “Noncontact SPO2 Measurement Using Eulerian Video Magnification.” IEEE Trans. on Instrumentation and Measurement, Vol. 69, No. 5, pp. 2120–30, 2019.

[18] J. Brieva, E. Moya-Albor, and H. Ponce. “A Non-Contact SpO2 Estimation Using a Video Magnification Technique.” 17th International Symposium on Medical Information Processing and Analysis, December 10, 2021.

[19] H. Lauridsen, S., Daniela Hedwig, K.L. Perrin, C.J. Williams, P.H. Wrege, M.F. Bertelsen, M. Pedersen, and J.T. Butcher. “Extracting Physiological Information in Experimental Biology via Eulerian Video Magnification.” BMC Biology 17, no. 1 (December 12, 2019).

[20] X. Fan, Q. Ye, X. Yang, and S.D. Choudhury. “Robust Blood Pressure Estimation Using an RGB Camera.” Jour. of Ambient Intelligence and Humanized Computing 11, no. 11 (September 4, 2018): 4329–36.

[21] E.E. Frezza and H.M. Mezghebe. “Indications and complications of arterial catheter use in surgical or medical intensive care units: analysis of 4932 patients.” The American surgeon 64 2 (1998): 127-31.

[22] J.J. Paik, R. Hirpara, J.A. Heller, L.K. Hummers, F.M. Wigley, and A.A. Shah. “Thrombotic Complications after Radial Arterial Line Placement in Systemic Sclerosis: A Case Series.” Seminars in Arthritis and Rheumatism 46, no. 2 (March 31, 2016): 196–99.

[23] B. Scheer, A. Perel, and U.J. Pfeiffer. “Clinical Review: Complications and Risk Factors of Peripheral Arterial Catheters Used for Haemodynamic Monitoring in Anaesthesia and Intensive Care Medicine.” Critical Care 6, no. 3 (April 18, 2002): 199–204.

[24] D. Shimbo, N.T. Artinian, J.N. Basile, L.R. Krakoff, K.L. Margolis, M.K. Rakotz, and G. Wozniak. “Self-Measured Blood Pressure Monitoring at Home: A Joint Policy Statement from the American Heart Association and American Medical Association.” Circulation 142, no. 4 (July 28, 2020): e42–63.

[25] T. Stogiannopoulos, G.A. Cheimariotis, and N. Mitianoudis. “A Study of Machine Learning Regression Techniques for Non-Contact SPO2 Estimation from Infrared Motion-Magnified Facial Video.” Information 14, no. 6 (May 23, 2023): 301.

[26] M. Rong, and K. Li. “A Blood Pressure Prediction Method Based on Imaging Photoplethysmography in Combination with Machine Learning.” Biomedical Signal Processing and Control 64 (February 2021): 102328.

[27] M. Yoshizawa, N. Sugita, M. Abe, A. Tanaka, N. Homma, and T. Yambe. “Non-Contact Blood Pressure Estimation Using Video Pulse Waves for Ubiquitous Health Monitoring.” 2017 IEEE 6th Global Conf. on Consumer Electronics (GCCE), December 21, 2017.

[28] R. Takahashi, K. Ogawa-Ochiai, and N. Tsumura. “Non-Contact Method of Blood Pressure Estimation Using Only Facial Video.” Artificial Life and Robotics 25, no. 3 (July 24, 2020): 343–50.

[29] R.H. Goudarzi, S.S. Mousavi, and M. Charmi. “Using Imaging Photoplethysmography (IPPG) Signal for Blood Pressure Estimation.” 2020 Int. Conf. on Machine Vision and Image Processing (MVIP), June 15, 2020.

[30] T. Hastie and R. Tibshirani, “Generalized Additive Models”, Statistical Science, Vol. 1, No. 3, Aug. 01, 1986.

[31] H. Shetty, and K. Pushpalatha, (2021) ”A cadaveric study of superficial palmar arch with surgical importance”, Journal of Clinical and Diagnostic Research, 15(9), pp. AC01–AC06.

[32] T. Stogiannopoulos, “Tomstog/Infrared-BP” GitHub, August 6, 2023. [Online]. Available: https://github.com/TomStog/Infrared-BP. [Accessed: 9-Sep-2023].